Geophysical Journal International

Geophys. J. Int. (2020) **223,** 1230–1246
Advance Access publication 2020 September 21
GJI Seismology

doi: 10.1093/gji/ggaa348

Inner core anisotropy measured using new ultra-polar PKIKP paths

Henry Brett and Arwen Deuss

Department of Earth Sciences, Utrecht University, 3584 CS Utrecht, The Netherlands. E-mail: h.brett@uu.nl

Accepted 2020 July 16. Received 2020 July 15; in original form 2020 February 5

SUMMARY

We measure the seismic anisotropy of the inner core using PKPbc-PKPdf and PKPab-PKPdf differential traveltimes, as a function of the angle ζ between the Earth's rotation axis and the ray path in the inner core. Previous research relied heavily on body waves originating in the South Sandwich Islands (SSI) and travelling to seismic stations in Alaska to sample inner core velocities with low ζ (polar paths). These SSI polar paths are problematic because they have anomalous travel time anomalies, there are no ultra-polar SSI paths with $\zeta < 20^\circ$ and they only cover a small part of the inner core. Here we improve constraints on inner core anisotropy using recently installed seismic stations at high latitudes, especially in the Antarctic, allowing us to measure ultra-polar paths with ζ ranging from 20°–5°. Our new data show that the SSI's polar events are fast but still within the range of velocities measured from ray paths originating elsewhere. We further investigate the effect of mantle structure on our data set finding that the SSI data are particularly affected by fast velocities underneath the SSI originating from the subducted South Georgia slab, which is currently located just above the core mantle boundary. This fast velocity region results in mantle structure being misinterpreted as inner core structure and we correct for this using a *P*-wave tomographic model. We also analyse the effect of velocity changes on the ray paths within the inner core and find that faster velocities significantly change the ray path resulting in the ray travelling deeper into the inner core and spending more time in the inner core. To remove this effect, we propose a simple but effective method to correct each event-station pair for the velocity-dependent ray path changes in the inner core, producing a more reliable fractional traveltime measurement. Combining the new ultra-polar data with mantle and ray path corrections results in a more reliable inner core anisotropy measurement and an overall measured anisotropy of 1.9–2.3 per cent for the whole inner core. This is lower than previous body wave studies (3 per cent anisotropy) and in better agreement with the value of inner core anisotropy measured by normal modes (2 per cent anisotropy). We also identify regional variation of anisotropic structure in the top 500 km of the inner core, which appears to be more complex than simple hemispherical variations. These regional variations are independent of the SSI data and are still present when these data are excluded. We also find a potential innermost inner core with a radius of 690 km and stronger anisotropy.

Key words: Body waves; Core; Seismic anisotropy.

1 INTRODUCTION

The inner core of the Earth is a challenging region to study. It was first discovered by Lehmann (1936) and is a solid sphere composed of an iron and nickel alloy with a radius of 1217.5 km (Kennett *et al.* 1995). The solidification of the inner core and the resulting release of latent heat drive convection in the outer core and thus sustains Earth's magnetic field (Gubbins *et al.* 2007). While geochemistry and mineral physics provide us with information about crystal structure and composition of the inner core, only seismology allows us to image the inner core and identify different structures within it (see Deuss 2014, Tkalčić 2015 and Romanowicz & Wenk 2017 for recent reviews). One of the most striking observations is that the inner core appears to be anisotropic, where the velocity of a seismic wave differs depending on the direction of wave propagation through a medium.

Anisotropy was first observed in the inner core by Poupinet *et al.* (1983) and they found that the traveltime of polar paths (ray paths with a $\zeta < 35^\circ$ where ζ is the angle between the ray path and the Earth's axis of rotation) was shorter than for equatorial paths ($\zeta > 35^\circ$). Morelli *et al.* (1986) quantified the inner core anisotropy explicitly, concluding that 1 per cent cylindrical anisotropy with the

fast direction aligned with Earth's rotation axis best explained the observed traveltime residuals. In the same year, Woodhouse *et al.* (1986) found that inner core anisotropy also explains observations of anomalous zonal splitting of Earth's free oscillations or normal modes.

The symmetry axis of anisotropy in the inner core has been a topic of research with early studies suggesting the axis is at an angle of 6°, relative to Earth's rotation axis (Shearer & Toy 1991; Creager 1992); later research placed the axis of anisotropy between 4° and 10° (Su & Dziewonski 1995; Song & Richards 1996; Isse & Nakanishi 2002). Irving & Deuss (2011) and more recently Frost & Romanowicz (2019) found that there was no evidence for a tilted anisotropy axis relative to the Earth's rotation axis.

There is also evidence for a heterogeneous distribution of inner core anisotropy into two hemispheres with different amounts of anisotropy (Tanaka & Hamaguchi 1997; Creager 1999; Garcia & Souriau 2000; Niu & Wen 2001; Garcia 2002; Wen & Niu 2002; Oreshin & Vinnik 2004; Yu & Wen 2006; Deuss *et al.* 2010; Irving & Deuss 2011; Lythgoe *et al.* 2014). A western hemisphere with slow isotropic velocity at shallow depths up to approximately 200 km and strong anisotropy deeper in the inner core was recognized, along with an eastern hemisphere with a fast isotropic velocity at shallow depth and little or no anisotropy at larger depths. The boundaries between these hemispheres vary significantly between the different studies and the term hemisphere is misleading as the eastern hemisphere is often found to be almost half the size of the western hemisphere. Thus, some research has started calling the hemispheres the quasi-western and quasi-eastern hemispheres (Tanaka & Hamaguchi 1997; Irving & Deuss 2011). Most evidence for hemispheres comes from body wave studies but normal modes have also observed the overall hemispherical pattern of anisotropy using cross-coupled splitting function observations (Deuss *et al.* 2010).

In addition to the lateral variations, there are also observed variations with depth. The uppermost 100 km of the inner core shows an isotropic slower layer in the west and a faster isotropic layer in the east (Niu & Wen 2001; Waszek & Deuss 2011). Some studies have also found evidence for an innermost inner core with a radius varying between 300 and 750 km, and a fast symmetry axis of anisotropy being oriented in the pseudo-equatorial plane and not showing hemispherical variations (Ishii & Dziewoński 2002; Beghein & Trampert 2003; Ishii & Dziewoński 2003; Sun & Song 2008a). The more recent body wave study by Lythgoe *et al.* (2014), however, does not observe an innermost inner core and proposes that observations of an innermost inner core are a result of averaging the hemispherical structure. Recent research by Frost & Romanowicz (2019) also shows that an innermost inner core is not required by their data but that if it did exist it would have a radius of 750 km and have an anisotropy axis quasi-parallel to Earth's rotation axis.

Table 1 summarizes previously published values of anisotropy and observations of hemispheres from body wave studies, while Table 2 does the same for normal mode studies for completeness. The value of inner core anisotropy found in previous body wave studies has an average value of 3 per cent and ranges between 0.7 and 5 per cent. The average value of anisotropy for normal modes from recent studies is 2 per cent and lower than the measurements from body wave studies.

The main problem faced by studies which measure inner core anisotropy from body waves has been the dominance of ray paths going from earthquakes in the South Sandwich Islands (SSI) to seismic stations in Alaska in polar data ($\zeta < 35°$) and the lack of ultra-polar data ($\zeta < 20°$). The SSI to Alaska ray paths are problematic as they have a much stronger positive traveltime anomaly than other polar ray paths (i.e. arrive earlier than expected). Due to the absence of ultra-polar data, the anisotropy models have been extrapolated for $\zeta < 20°$ leading to anisotropy values of up to 5 per cent for body waves (see Table 1). The anisotropy from body waves has also been difficult to reconcile with much smaller normal mode anisotropy values of only 2 per cent.

The source of the positive traveltime anomaly from the SSI has been the subject of many previous studies. One of the earliest studies to draw attention to these ray paths was Romanowicz *et al.* (2003), who conducted corrections using mantle tomography models on the SSI to Alaska ray paths. They concluded that while some of the anomaly could be explained by mantle structure a significant source of the anomaly was necessary somewhere in the core. They proposed an 'outer core tangent cylinder' with a positive *P*-wave velocity anomaly of 1 per cent as an explanation for the SSI anomaly. This cylindrical structure which is tangent to the inner core and parallel to Earth's axis of rotation was proposed by outer core geodynamical modelling (Hollerbach & Jones 1995; Olson *et al.* 1999). Tkalčić (2010) took a different approach and analysed PcP paths originating from the SSI. He found that these lower mantle phases with no sensitivity to the inner core, also exhibit strong positive traveltime anomalies of the same order as that observed in the inner core. He concluded that the source of the traveltime anomaly could be due to mantle structure beneath the SSI. Long *et al.* (2018) proposed that a lower mantle structure with a small size of only a few hundreds of km underneath Alaska could explain the anomaly and would not show up easily on global tomographic models due to its small size. Most recently, the work of Frost *et al.* (2020), using array techniques in Alaska and 3-D ray tracing, shows that the Alaskan slab has a profound effect on the arrival times of the PKPdf phase, implying that the SSI anomaly is due to upper-mantle effects on the Alaskan side of the SSI to Alaska ray paths.

The recent installation of new Antarctic seismic stations and a complete reanalysis of all suitable data available through the International Federation of Digital Seismograph Networks (FDSN) has made it possible to observe ultra-polar paths and significantly increase the number of polar events which do not have an origin in the SSI region. In this paper, we will present a new large body wave data set of PKPdf-PKPbc and PKPdf-PKPab differential traveltimes with more polar and ultra-polar paths than previously published. The new data allows us to improve constraints on inner core anisotropy and to constrain the SSI anomaly. We also propose a simple method to correct differential traveltime measurements for the fact that corresponding velocity anomalies lead to a shallower or deeper ray path in the inner core. In addition, we also correct for the significant influence of heterogeneous mantle structure, as imaged through tomography, on our data. Combining the new data with ray path and mantle corrections greatly improves the longitudinal and depth resolution of the inner core and gives us greater insight into inner core structure. It also removes the need for using the South Sandwich Island ray paths and allows us to investigate anisotropy without using these data.

2 METHODOLOGY

2.1 Data collection and processing

We measure inner core anisotropy with compressional body waves, using the arrival time of the PKPdf phase (which travels through

Table 1. Summary of values of anisotropy from previous body wave studies, note that this list is not exhaustive. Some papers that propose hemispheres but do not explicitly state values of anisotropy, likewise some papers do not mention hemispheres at all, thus a lack of 'yes' under column 'Hemispheres' does not mean that those authors conclude that hemispheres do not exist. Some papers do not explicitly state their measured values of anisotropy and it has to be inferred. Papers that only used PKPcd as a reference phase and therefore focused on the upper most inner core have been left out.

Author	Year	Reference phases	Anisotropy overall	Hemispheres	Eastern anisotropy	Western anisotropy
Poupinet et al.	1983	P	–	–	–	–
Morelli et al.	1986	PKPbc, PKPab	1.0%	–	–	–
Shearer et al.	1988	PKPbc	3.0%	–	–	–
Shearer and Toy	1991	PKPbc	4.0%	–	–	–
Creager	1992	PKPbc	3.5%	–	–	–
Tanaka and Hamaguchi	1997	PKPbc	1.5%	Yes	0.5%	2.4%
Creager	1999	PKPbc, PKPab	2.0%	Yes	0.5%	2–4%
Garcia and Souriau	2000	PKPbc	3.0%	–	–	–
Garcia	2002	PKPbc, PKPab	3.0%	Yes	–	–
Garcia et al.	2006	PKPbc, PKPab	–	Yes	–	–
Sun and Song	2008	PKPbc, PKPab, PKPcd	2.0%	Yes	0.5%	2.0%
Leykam et al.	2010	PKPbc, PKPab	0.7%	Yes	0.1%	–
Irving and Deuss	2011	PKPbc, PKPab	3.5%	Yes	1.4%	4.5%
Lythgoe et al.	2014	none	5%	Yes	0.5–1.5%	3.5–8%
Frost and Romanowicz	2019	PKPbc, PKPab, PKIIKP-PKPdf2	3.5%	Yes	–	–

Table 2. Summary of values of anisotropy from normal mode studies of the inner core.

Author	Year	Anisotropy overall
Woodhouse et al.	1986	3.35%
Tromp	1993	2.1%
Durek and Romanowicz	1999	2.50%
Ishii et al.	2002	1.75%
Beghein and Trampert	2003	2.94
Mäkinen et al.	2014	1.75%

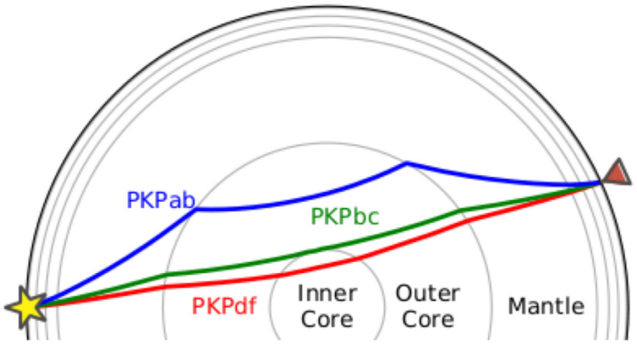

Figure 1. Ray paths of PKPdf (red), KPab (blue) and PKPbc (green) phases through the Earth, made using Obspy and TauP. The star represents the location of the source and the triangle is the location of the seismometer that measures the arrivals.

the mantle, outer core and inner core) in comparison to the arrival time of the PKPbc and PKPab phases (which only travel through the outer core and the mantle), see Fig. 1 for their ray paths. Event-station pairs were collected for stations available through the FDSN recording between 1991 and 2019 with an epicentral distance between 146.5° and 178° and an event body wave magnitude greater than $m_b = 5.0$. These seismograms are then bandpass filtered with two poles and corner frequencies at 0.5 and 2 Hz. We inspected the vertical component seismograms for 188 257 event-station pairs by eye and from this selected a high-quality data set of 2186 seismograms (a pass rate of 1.24 per cent). The pass rate is so low due to the high attenuation of the PKPdf phase; this means that this phase is not visible above the noise threshold in the majority of seismograms.

We measure the traveltime difference between PKPdf and PKPab or PKPbc to minimize the effect of mantle structure and inaccuracies in event location and time (Creager 1992). The difference in arrival times between these phases has been assumed to be caused by inner core structure alone. This assumption is based on the argument that the inner core (PKPdf) and outer core phases (PKPbc and PKPab) travel nearly the same path through the Earth, deviating only in the inner core. Looking at Fig. 1, it can be seen that this assumption is more valid for PKPbc than PKPab. We will investigate if this assumption is indeed correct in Section 3.2.1 and will show that especially for the SSI this may not be the case. The PKPbc-PKPdf differential traveltime is measured for epicentral distances between 146° and 155.5° while the PKPab-PKPdf differential traveltime is measured for epicentral distances between 150° and 180°. As a result, PKPbc-PKPdf is only sensitive to the upper 350 km of the inner core while the PKPab-PKPdf differential traveltime is sensitive to up to 1100 km below the inner core boundary (allowing sampling of almost the entire volume of the inner core).

Using our measured arrival times, we calculate the differential traveltime δt;

$$\delta t = (t_{\mathrm{PKPref}} - t_{\mathrm{PKPdf}})_{\mathrm{data}} - (t_{\mathrm{PKPref}} - t_{\mathrm{PKPdf}})_{\mathrm{AK135}}, \quad (1)$$

where $(t_{\mathrm{PKPref}} - t_{\mathrm{PKPdf}})_{\mathrm{data}}$ is the difference in arrival time between a reference phase (either bc or ab) and the PKPdf phase, as measured in the data. The second term, $(t_{\mathrm{PKPref}} - t_{\mathrm{PKPdf}})_{\mathrm{AK135}}$, is the difference in arrival time as predicted by the 1-D model AK135 (Kennett *et al.* 1995) and calculated using the TauP toolkit (Crotwell *et al.* 1999). Differential traveltimes are corrected for ellipticity using the method of Dziewonski & Gilbert (1976).

We define the angle ζ between the ray path in the inner core and the Earth's rotation axis as

$$\cos(\zeta) = \frac{\cos(\theta_o) - \cos(\theta_i)}{\sqrt{2 - 2\cos(\theta_o)\cos(\theta_i) - 2\sin(\theta_o)\sin(\theta_i)\cos(\phi_o - \phi_i)}}, \quad (2)$$

where θ_o and θ_i are the co-latitudes of where the ray leaves and enters the inner core while ϕ_o and ϕ_i are the longitudes (i.e. Irving & Deuss 2011). The pierce point locations (where the PKPdf ray

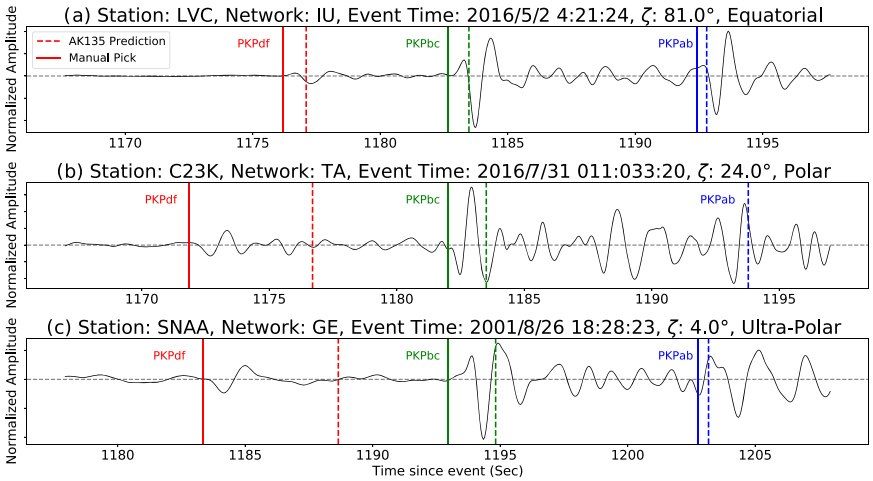

Figure 2. Three seismograms of different values of ζ showing PKPdf (red), PKPbc (green) and PKPab (blue) phases. The solid lines are the arrivals picked by hand while the dashed lines are the arrivals of each phase as predicted by AK135 (Kennett *et al.* 1995) and is calculated using the TauP toolkit (Crotwell *et al.* 1999).

Table 3. Numbers of differential traveltimes collected for each phase and corresponding range of ζ. For some events both PKPab and PKPbc have been measured, for other events only one of the two phases has been measured. The 'Total' column gives the total number of unique ray paths, that is, $N_{\text{ab \& bc}} + N_{\text{only ab}} + N_{\text{only bc}}$.

ζ	ab & bc	Only bc	Only ab	Total
All ζ	742	821	623	2186
$\zeta > 35$	350	268	468	1086
$20 < \zeta < 35$	338	498	120	956
$\zeta < 20$	54	55	35	144

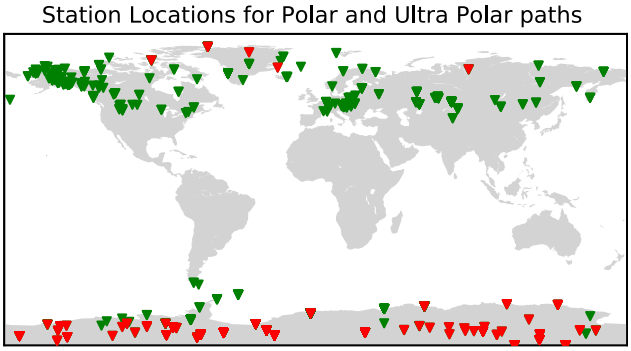

Figure 3. Map of the station locations used to measure polar data (green triangles) and ultra-polar data (red triangles).

enters and leaves the inner core) are calculated using the AK135 model (Kennett *et al.* 1995) and the TauP toolkit (Crotwell *et al.* 1999) in combination with the python package 'Geographicslib'. If a ray path has $\zeta > 35°$, we call it an equatorial path, if it has $\zeta < 35°$ it is polar and if a ray path has $\zeta < 20°$ it is considered ultra-polar.

Fig. 2 shows three example seismograms and the phase arrival times predicted by AK135 and our own picks. To measure the arrivals we pick the times of the onset of each phase, minimizing the effect of attenuation in the inner core which causes the PKPdf peak to be broadened relative to the PKPbc and PKPab arrivals. It can be seen that the PKPdf phase arrives approximately when predicted by AK135 on the equatorial seismogram (Fig. 2a) but for the polar path (Fig. 2b) and ultra-polar path it arrives much earlier (Fig. 2c). These traveltime anomalies are evidence for anisotropy with the fast axis in the polar direction.

For 742 seismograms in our data set it is possible to measure all three phases (such as Figs 2a and c). By comparing the differential traveltimes measured using PKPab and PKPbc for the same seismogram (see Supporting Information Fig. S1 and explanation) we get a rough estimate of errors using the differential traveltime methodology, although this is restricted to the epicentral distance range of 146°–155.5° due to the PKPbc phase. We find that the PKPab and PKPbc are correlated but that there is some scatter which reflects the measurement error. The uncertainty in the PKPab differential traveltimes for larger epicentral distances will be greater, as demonstrated by Brëger *et al.* (2000) and Garcia *et al.* (2006).

One of the key aims of this research is to significantly increase the currently available data sets of PKPdf-PKPbc and PKPdf-PKPab paths, particularly focusing on extending the observations of polar paths and earthquakes not originating in the SSI. Our aim was largely achieved through the re-collection and re-analysis of all polar data available from the FDSN since 1991 and resulted in a data set of 2186 high-quality seismograms of which 623 PKPbc (only), 821 PKPab (only), and 742 have both PKPab and PKPbc measurements (see Table 3). 584 measurements are polar paths which do not originate in the SSI and of these 142 paths are ultra-polar. This new polar data was largely collected from stations at high latitudes, especially the Antarctic; Fig. 3 shows the locations of these stations. Leykam *et al.* (2010) were the first to recognize the potential of using these new high-latitude seismic stations to better constrain inner core anisotropy. However, since Leykam *et al.* (2010) many more earthquakes have been recorded and yet more seismic stations installed at high latitudes allowing for a significant increase in ultra-polar data. For example, Leykam *et al.* (2010) measured 17 PKPdf-PKPab and PKPdf-PKPbc ultra-polar paths in comparison to 144 in our study (Table 3). Revisiting this data is significant as our values of anisotropy for the inner core are much higher than those of Leykam *et al.* (2010) as a result of the increased data coverage.

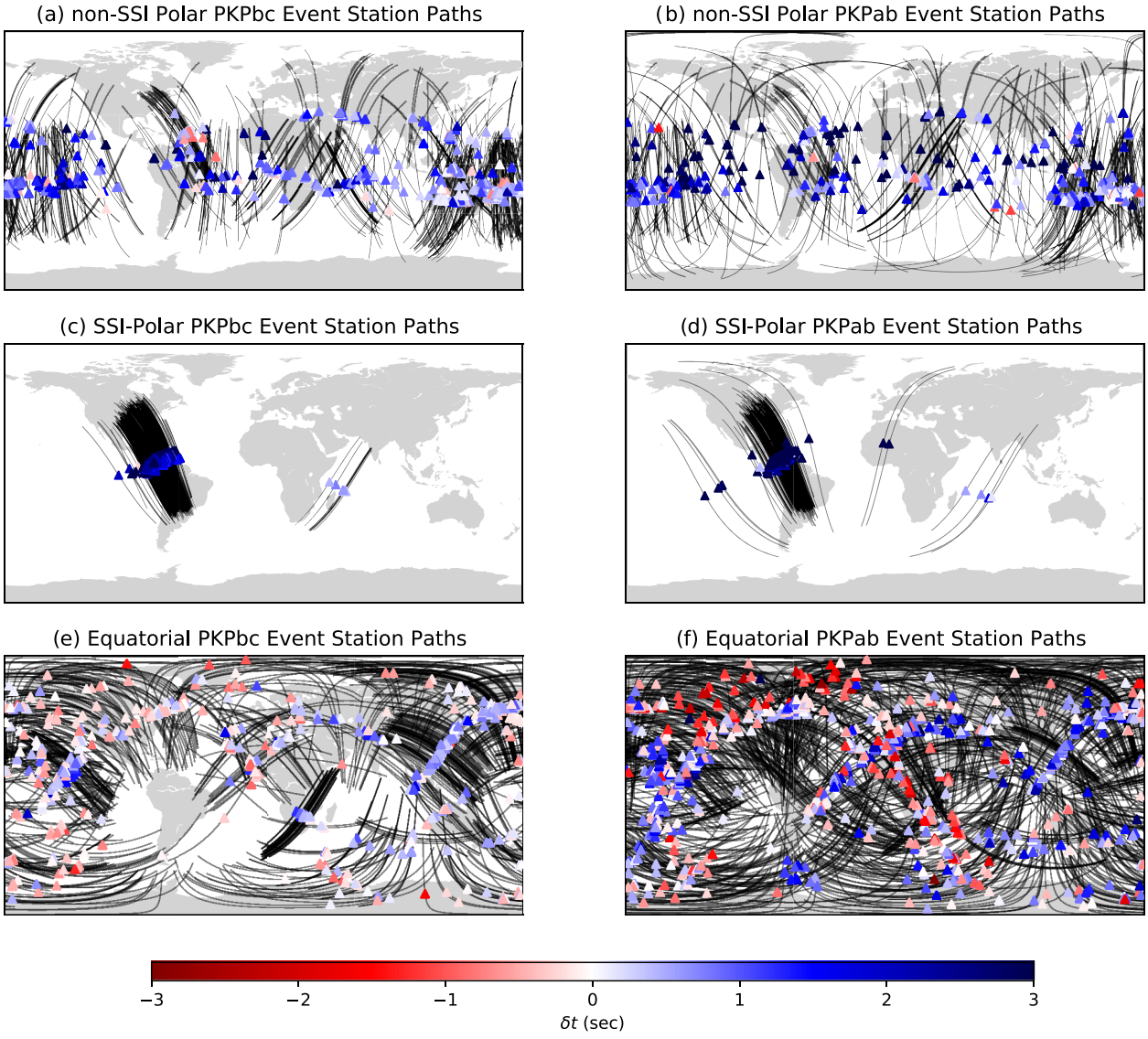

Figure 4. The global coverage of our data set with the left-hand column being data with PKPbc as the reference phase and the right-hand column with PKPab as a reference phase. (a and b) Ray path coverage within the inner core of polar data excluding the SSI, (c and d) of equatorial data and (e and f) ray path coverage of SSI data. The colour of the triangles indicate the δt of each ray path and are plotted at the location of the turning point of the ray path.

Data utilizing these new Antarctic seismic stations have also been used to investigate inner core anisotropy in the recent paper by Frost & Romanowicz (2019), however the data set we present here has been collected independently and includes different event station pairs.

3 RESULTS

3.1 Anisotropy

A medium is said to be anisotropic when seismic velocity is dependent on the direction of wave propagation through the medium. To accurately measure anisotropy, it is important to have differential traveltime (δt) data with a good global coverage for all angles of ζ and spanning all longitudes. Fig. 4 shows the spatial sampling of our data set, and includes good even coverage of polar data which do not have an origin in the SSI (Figs 4a and b) due to our extensive use of stations in the Antarctic (Fig. 3). Our data set represents a significant improvement in data coverage on previous research. Looking at the δt of all the paths it can be seen that polar paths have mostly positive δt (i.e. faster) paths but that there are also examples of polar ray paths with negative δt (i.e. slower). There are more equatorial paths with negative δt than polar paths, but there are also regions of equatorial paths with positive δt (Figs 4e and f). The polar paths for events originating in the SSI, have the strongest positive δt anomalies and high numbers of paths traveling to Alaska can be seen (Figs 4c and d). These are the paths which have dominated inner core anisotropy measurements for so long due to their high number and strong positive anomaly; they are the reason why finding more polar and ultra-polar data not originating in the SSI is important.

Fig. 5 shows how $\delta t/t$ varies with ζ for our data set. $\delta t/t$ is the differential traveltime δt calculated using eq. (1) normalized by the time spent in the inner core (t) as modelled using AK135. This

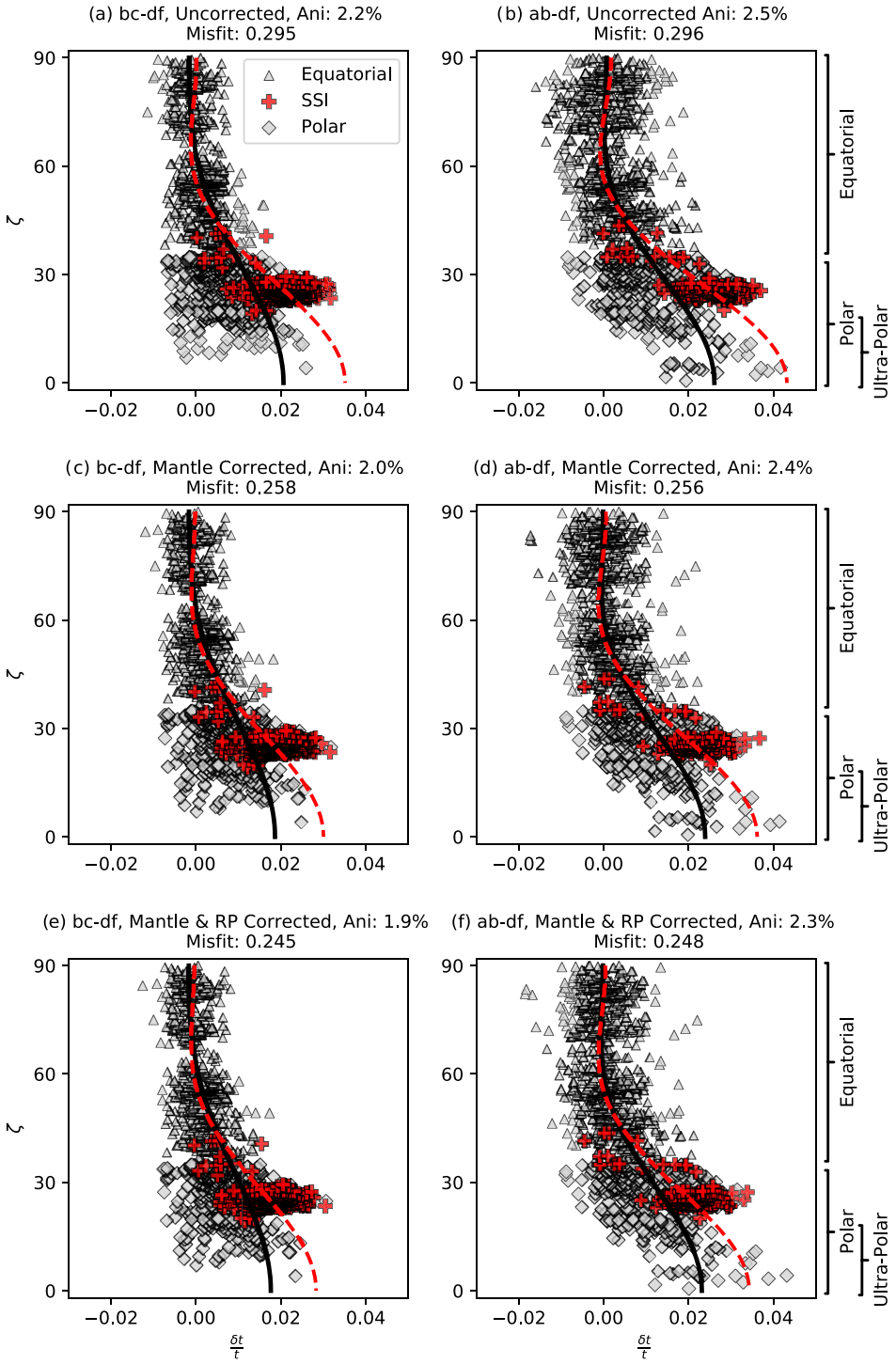

Figure 5. (a) Variation of $\delta t/t$ as a function of ζ for (a) PKPbc-PKPdf and (b) PKPab-PKPdf. The black line is the function described by eq. (3) fitted to all data with a least-squares norm. The black dashed line is the function described by eq. (3) fitted to equatorial and SSI data only. The triangles are equatorial data ($\zeta > 35^\circ$), diamonds are polar data (not including SSI) and the crosses are the SSI data. (c and d) Variations of $\delta t/t$ against ζ applying mantle corrections using the UUP07 tomographic model. (e and f) Variation of $\delta t/t$ applying mantle and ray path corrections.

normalization takes into account the different amount of time travelled by rays going deeper or shallower through the inner core. Ray paths with smaller values of ζ have a stronger positive traveltime anomaly than equatorial paths with larger values of ζ, albeit with a large scatter (Figs 5a and b). The SSI data clearly stand out when compared to other polar data, and unfortunately no ultra-polar data exists for earthquakes originating in the SSI. Supporting Information Fig. S2 shows the same figures without the SSI data further highlighting the influence of these data.

To measure anisotropy from our data we need to quantify the change in velocity as a function of ζ so that we can relate it to the relevant components of the elastic tensor. We model anisotropy

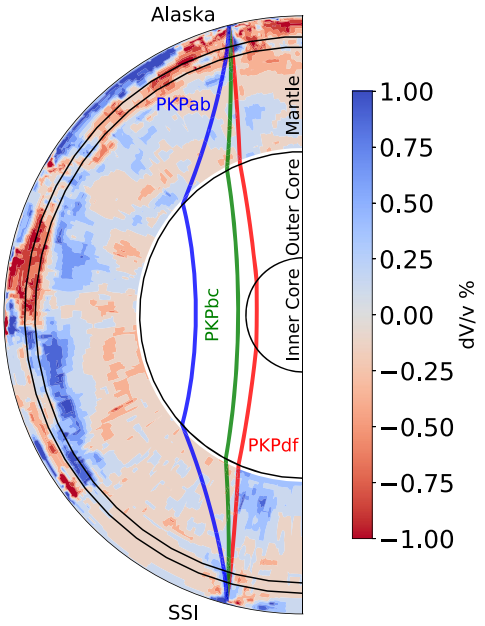

Figure 6. A cross-section through the UUP07 model by Amaru (2007).

using the same equation as in previous research (i.e. Creager 1992, 1999; Poupinet *et al.* 1983; Irving & Deuss 2011; Lythgoe *et al.* 2014):

$$\frac{\delta t}{t} = \frac{\delta v}{v} = a + b\cos^2(\zeta) + c\cos^4(\zeta), \tag{3}$$

where $\delta t/t$ is equivalent to the velocity anomaly $\delta v/v$ assuming low attenuation in the inner core, and a, b and c are the Love coefficients (Love 1927). The isotropic velocity perturbation is given by a and $b + c$ describes the anisotropy (Creager 1999). The b and c parameters of eq. (3) can be related to components of the elastic tensor which describes the anisotropy of a medium, that is, $b = (C_{33} - C_{11})/2C_{11}$ and $c = (4C_{44} + 2C_{13} - C_{11} - C_{33})/8C_{11}$ (Creager 1992). By fitting eq. (3) to our data set of measured $\delta t/t$, we determine the a, b and c parameters and relate these to velocity anisotropy.

When we fit eq. (3) to our whole data set (including the SSI and our new ultra-polar data), we get an average anisotropy for the inner core of 2.5 per cent for PKPdf-PKPab and 2.2 per cent for PKPdf-PKPbc. These values are lower than measurements from other body wave studies which normally find values of 3–4 per cent. Our lower anisotropy values are a direct result of having more polar data and especially ultra-polar data ($\zeta < 20°$). If we fit eq. (3) only to the equatorial data and data from the SSI, then we get a much larger anisotropy of 3.5 per cent for PKPbc and 4.2 per cent for PKPab. Without the ultra-polar data, the anisotropy will be extrapolated from the SSI anomalies for $\zeta < 25°$ resulting in an overestimation of anisotropy. This is why ray paths travelling from the SSI to stations in Alaska became the focus of much debate (Tkalčić 2015) and explaining the large positive velocity anomaly arising from the South Sandwich Island data is a key challenge in measuring inner core anisotropy.

3.2 The SSI

While the traveltime anomalies $\frac{\delta t}{t}$ for the SSI to Alaska ray paths are within the spread of other polar data, the source of the fast velocities is still an important question. After inspection of over 186 359 seismograms, we found that the SSI data had some of the clearest arrivals and were relatively easy to measure differential traveltimes. This leads to the conclusion that the observed PKPbc/ab-PKPdf measurements for the SSI are accurate, ruling out systematic measurement error. Thus, there seems to be three possible explanations for the large SSI $\delta t/t$:

(1) Mantle and outer core heterogeneity is affecting the arrival times of PKPdf/bc/ab phases unequally.
(2) Our modelled ray paths are inaccurate.
(3) The SSI $\delta t/t$ is an accurate measurement of the inner core and there is a large positive velocity anomaly along the SSI to Alaska ray paths.

3.2.1 *Mantle heterogeneity*

When we use differential arrival times to investigate inner core structure we assume that PKPdf and the reference phases PKPbc and PKPab sample the same structure in the mantle and that the outer core is laterally homogeneous. If this assumption is incorrect it would result in mantle structure being misinterpreted as inner core structure. Looking at Fig. 1 it can be seen that there are large differences between the PKPab and PKPdf ray paths in the lower mantle and outer core while the ray paths travel much closer in the upper mantle. This is also reflected by the PKPbc ray paths but the differences are smaller. If mantle heterogeneity is indeed affecting the differential traveltime measurements then it will most likely occur in the lower mantle because this is where the PKPbc and PKPdf ray paths differ most. However we cannot rule out upper-mantle structure.

To investigate whether the PKPab, PKPbc and PKPdf phases sample different structure in the lower mantle we use the UUP07 mantle P-wave tomographic model from Amaru (2007). A cross-section through the UUP07 model going from the SSI to Alaska (Fig. 6) shows that underneath the SSI, there is a strong positive velocity anomaly interpreted to be the subducted South Georgia slab (van der Meer *et al.* 2018). The PKPdf phase appears to just pass through this faster material underneath the SSI, while the PKPbc and PKPab phases do not. Thus, mantle structure does affect PKPbc, PKPab and PKPdf differently.

We correct for our whole data set for mantle structure using UUP07, including the SSI data and non-SSI data (Figs 5c and d). This is done using 1-D rays calculated for AK135 and then integrating the velocity anomaly from the tomographic model over the entire path of the ray. While taking into account 3-D effects would be a more thorough approach, doing this for a global dataset and global tomographic model is not straightforward and considered as a subject for future study. Initially the effect appears minor, only reducing the anisotropy for PKPbc-PKPdf to 2 per cent (Figs 5b and d) and for PKPab-PKPdf to 2.4 per cent (Figs 5a and c). However, a closer look reveals that the SSI data is more strongly affected compared to the rest of the data. Furthermore the misfit (calculated using an L2 norm), shown in the title of each panel on Fig. 5 is reduced in both the PKPbc and PKPab data by these corrections. Doubling or tripling the UUP07 corrections reduces the $\frac{\delta t}{t}$ anomaly from the SSI significantly, while the rest of the data experiences much lower $\delta t/t$ reductions (Fig. 7). The choice of doubling or tripling the velocities in the UUP07 model is chosen only to get a first order estimate of the magnitude of the velocity anomalies necessary. Tripling UUP07 corrections moves the SSI measurement to be much more similar to the non-SSI data and brings them into better agreement. This can be seen by comparing the black and grey dashed lines in Figs 7(e) and (f), which represent function (3) fitted to all the data (black

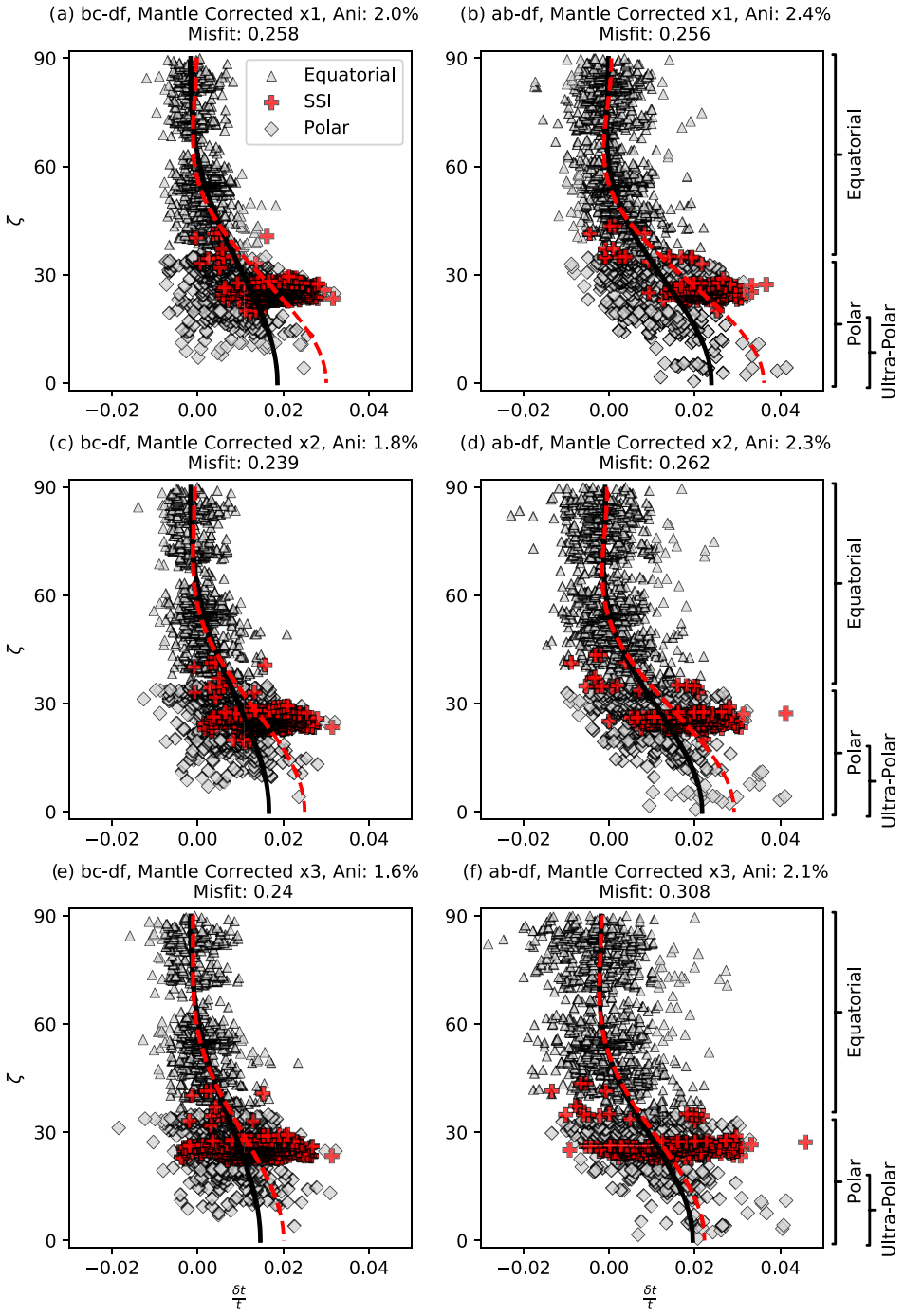

Figure 7. Variation of $\delta t/t$ as a function of ζ for (a) PKPbc-PKPdf and (b) PKPab-PKPdf with mantle corrections using the UUP07 model. The black line is the function described by eq. (3) fitted to all data with a least-squares norm. The black dashed line is the function described by eq. (3) fitted to equatorial and SSI data only. The triangles are equatorial data ($\zeta > 35^\circ$), diamonds are polar data (not including SSI) and the crosses are the SSI data. (c and d) Variations of $\delta t/t$ against ζ applying mantle corrections using the UUP07 tomographic model but with amplitudes x2. (e and f) Variation of $\delta t/t$ applying mantle corrections using the UUP07 tomographic model but with amplitudes x3.

line) and only the equatorial and SSI data respectively (grey dashed line). The PKPbc-PKPdf anisotropy reduces to 1.6 per cent and the PKPab-PKPdf to 2.1 per cent when UUP07 amplitudes are tripled. It may be an oversimplification to simply scale the amplitudes of UUP07, but it is well known from full-waveform inversion studies that ray based traveltime tomography significantly underestimates the amplitudes of velocity anomalies in the lower mantle. It can be seen on Fig. 7 that doubling or tripling the tomographic velocity anomalies decreases the overall misfit of the bc-df data, but increases the misfit for the ab-df data. It is likely that such magnitude of change is reasonable for the SSI region, but a bad fit for the rest of the data. Further work is required to quantify and isolate this effect, so for the rest of the paper we shall primarily consider data with mantle corrections x1.

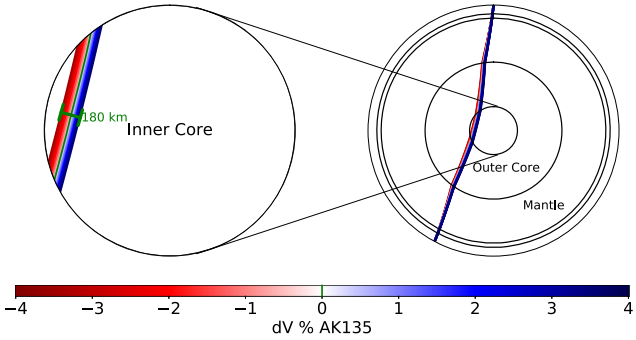

Figure 8. Different ray paths for a distance of 152° with the green path being the path modelled by AK135, the red paths are slower by up to −4 per cent and the blue paths are faster by up to +4 per cent of overall AK135 inner core velocity.

It is interesting to note that two recent papers, Long *et al.* (2018) and Frost *et al.* (2020), analysed the SSI to Alaska ray paths and also found that mantle structure was influencing the SSI data significantly. Long *et al.* (2018) showed that a small anomaly at the base of the mantle on the Alaskan side could cause the SSI traveltime anomaly, while Frost *et al.* (2020) propose that the SSI data is affected by the slab underneath Alaska. While our mantle corrections do not find that the PKPdf, PKPbc and PKPab phases experience different velocities under Alaska we certainly do not rule it out because we are using a global tomography model to correct our entire data set and not a high-resolution local model under Alaska to specifically look at the SSI to Alaska ray paths. Indeed it seems possible that a combined influence from the Alaska and South Georgia slabs could be at the heart of the anomalous traveltimes and in the future it will be important to conduct full-waveform tomography on the region covered by the SSI to Alaska ray paths.

In either scenario, this research does cast doubt on interpreting the SSI traveltime anomalies as inner core structure because they may be severely affected by mantle structure.

3.2.2 Ray path corrections

The PKPdf ray path in the inner core changes significantly when the inner core velocity is varied by ±5 per cent for an epicentral distance of 152° (the average of the SSI to Alaska paths), see Fig. 8. Increasing the inner core velocity by 4 per cent results in a ray path which travels 75 km deeper into the inner core. The corresponding inner core traveltime, t, increases by 10 s (Fig. 9b). Only ray paths with a small epicentral distance are severely affected, because at very large epicentral distances (>170°) it is not possible to find a faster path through the inner core by travelling deeper. The ray paths from the SSI to Alaska have small epicentral distance, so they are most severely affected.

We propose a new method to determine $\delta t/t$, incorporating the change in t due to the velocity change. The traditional method of measuring fractional traveltime, as described in eq. (1), involves measuring an observed value of differential traveltime: PKPref-PKPdf (shown as the horizontal red dashed line in Fig. 9a) and then finding the difference with the AK135 prediction (the blue dashed line) and dividing this by the inner core traveltime as predicted by AK135. Instead, we find the uniform per cent change in AK135 inner core velocity (i.e. no scaling with depth) required to fit the observed differential arrival time δt and use that to calculate a new ray path and corresponding inner core traveltime t_{corr} and use this new inner core traveltime to calculate $\delta t/t_{corr}$ instead of $\delta t/t_{AK135}$. The newly calculated t_{corr} changes the differential traveltime measurement $\delta t/t_{corr}$ by a maximum of 13.5 per cent (Figs 5e and f) which is enough to decrease the overall anisotropy measurement by 0.1 per cent for both PKPab and PKPbc data sets to 1.9 and 2.3 per cent, respectively. This correction depends greatly on the magnitude of the δt measurement and the epicentral distance. The effect is greater for smaller epicentral distances and becomes insignificant for epicentral distances greater than 155°. It is interesting to note that the data from the SSI are more affected than other data because they have a large δt measurement and relatively small epicentral distance.

Another approach than the one described above is also possible where the velocity model and ray path are updated iteratively until convergence is reached, this produces identical results across all values of distance and δt as our methodology.

Sun & Song (2008b) also identified the problem that the ray path changes as a function of inner core velocity. They used the adaptive ray bending method from Koketsu & Sekine (1998) to incorporate the ray path changes in tomographic modelling, and requires significant numerical modelling. Our approach is very simple and can be easily and effectively applied to data measurements without requiring intensive computer modelling or ray tracing.

3.2.3 The SSI data are accurate

There is an alternative explanation which should not be ruled out: that the SSI anomaly is a consequence of real inner core structure. There are some merits to this idea. Indeed, the differential traveltime methodology, despite the pitfalls discussed in Section 3.2.1, is a tried and tested methodology in seismology for removing event mislocation effects and mantle and outer core structure. Furthermore it cannot be denied that the SSI anomaly is a robust observation; there is no polar path in the inner core better sampled than the SSI to Alaska ray paths. Furthermore, there have been multiple attempts to isolate and identify the root cause of the SSI anomaly outside of the inner core and while the analysis in recent years are improving (Frost *et al.* 2020; Long *et al.* 2018), none (including this paper) have yet been totally conclusive. The consequence of accepting the SSI anomaly as a product of inner core anisotropy is that it requires anisotropy in the inner core within a (relatively) small region to be 4 per cent or greater and an increased level of heterogeneity.

4 INNER CORE STRUCTURE

Having corrected for mantle velocity anomalies using UUP07 and ray path changes in the inner core (Figs 5e and f), we investigate how our new data set constrains inner core structure. While our data doesn't show large variations in anisotropy with latitude, it does show variations with longitude and depth. The analysis here is an initial estimate and the basis from which we will conduct more rigorous modelling in future papers.

4.1 Variations with longitude

A first-order observation made by multiple other studies is the stronger anisotropy in the 'western' hemisphere than in the 'eastern' hemisphere at depths greater than approximately 200 km

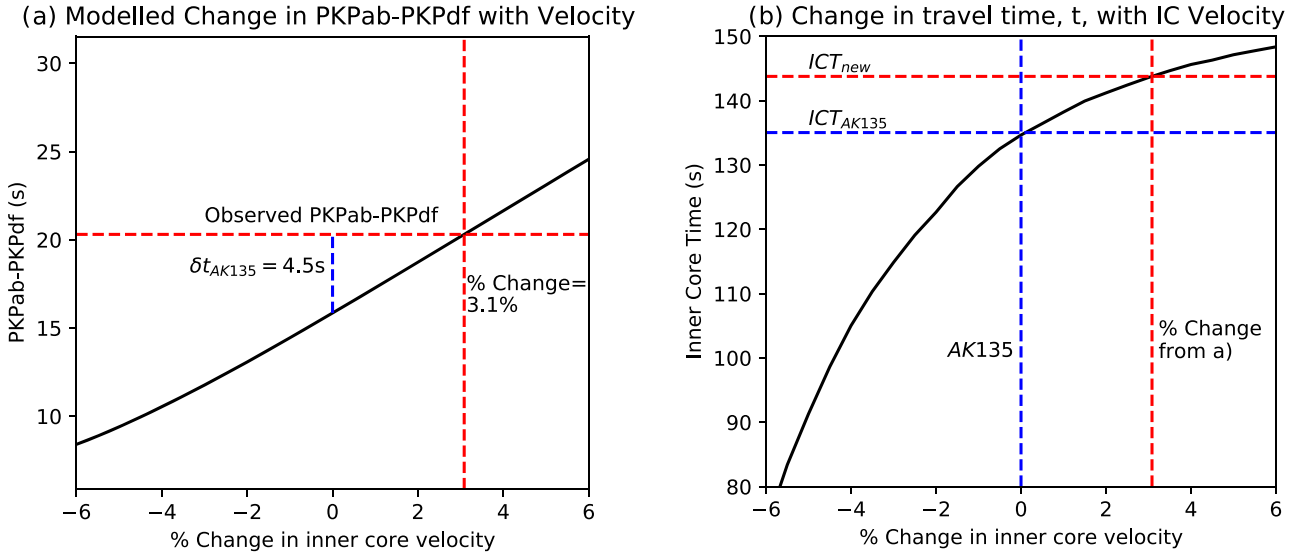

Figure 9. A visual explanation of the ray path corrections for an event originating in the SSI at 2016 July 31 and going to station COLD in the AK network with an epicentral distance of 152°. (a) Predicted PKPab-PKPdf differential time, relative to AK135, as a function of increased or decreased inner core velocity (solid black line). The horizontal red dashed line shows the observed PKPab-PKPdf differential traveltime. The vertical red dashed line indicates which percentage increase in inner core velocity best fits the observed PKPab-PKPdf. The vertical blue dashed line shows the δt that would be calculated using AK135 inner core velocities. (b) Effect of increasing or decreasing inner core velocity on time spent in the inner core (solid black line). For our example event and epicentral distance, the AK135 predicted inner core traveltime is indicated by dashed blue lines, and the corrected inner core traveltime value calculated by taking the 3.1 per cent change found in (a) is shown by the dashed red lines.

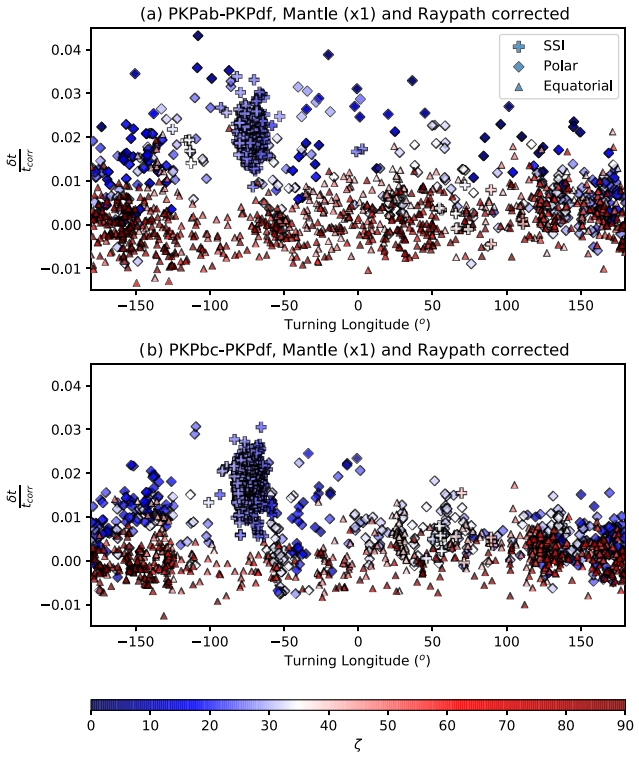

Figure 10. Values of $\delta t / t_{\mathrm{corr}}$ plotted against the longitude of the inner core turning point for the mantle corrected (UUP07 amplitudes x1) and ray path corrected data for (a) the PKPab-PKPdf data and (b) the PKPbc-PKPdf data. Triangles are equatorial data, diamonds are polar data not including the SSI and crosses are the data from the SSI. The colour shows the value of ζ for each data point where blue is polar and red is equatorial.

(Tanaka & Hamaguchi 1997; Creager 1999; Garcia & Souriau 2000; Garcia 2002; Niu & Wen 2001; Wen & Niu 2002; Oreshin & Vinnik 2004; Yu & Wen 2006; Deuss *et al.* 2010; Irving & Deuss 2011; Waszek & Deuss 2011; Lythgoe *et al.* 2014). The hemispherical variation in anisotropy is also visible in our data with polar paths being faster than equatorial paths in the west while in the east there is a smaller difference in traveltime between polar and equatorial paths (Fig. 10).

To quantitatively define boundaries between regions of different anisotropy and test the resolution of the inner core that can be achieved with our data, we compute a value of anisotropy for overlapping windows of fixed longitude width (Fig. 11). We fit eq. (3) to a subset of the data defined by a window of a fixed width centred around a specific longitude. For example, the anisotropy centred at longitude 0° with a window width of 180° is defined by determining the anisotropy for all the data between 90°W and 90°E defined by their turning point location. We then move this window by 1° across all the longitudes. This allows us to test for structures on different scales. Hemispheres, which are thought to split the inner core approximately in half, are investigated by using a width of 180° (Fig. 11a). We confirm previous studies and find stronger anisotropy of two to three per cent in the west and only 1–1.5 per cent in the east. Even when we increase the mantle corrections to x2 or x3, or when we leave out the SSI data, still we find stronger anisotropy in the west than in the east. The mantle corrections do, however, significantly reduce the magnitude of the western hemisphere's anisotropy from 3 to 2 per cent, while not changing the anisotropy in the east. Fig. 11(a) shows reductions in anisotropy around longitudes 60°W and 120°E representing the best locations for the hemisphere boundaries.

Decreasing the window width will lead to an increase in longitudinal resolution, but at the same time decreases the amount of data in each window and therefore increasing the uncertainty in the anisotropy calculation. We choose to limit our window widths so

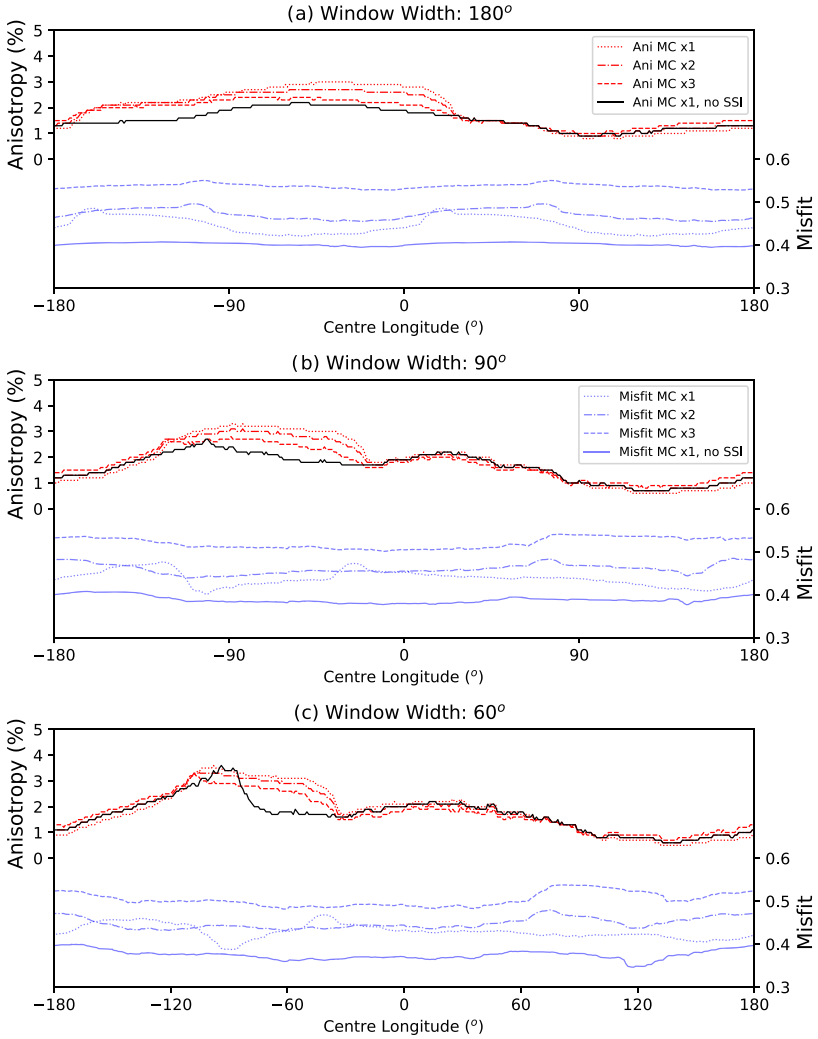

Figure 11. Anisotropy measured within a window of longitudes with window widths of (a) 180° , (b) 90° and (c) 60°. Each window panel shows results from data with mantle corrections (MC) with 1x, 2x, 3x UUP07 amplitudes and 1x UUP07 amplitudes but no data from the SSI. The L2 misfit is shown in blue for data with MC with 1x, 2x, 3x UUP07 amplitudes and 1x UUP07 amplitudes but no data from the SSI. All ray paths have been corrected for faster inner core velocities.

that no subset of data can have less than 50 polar data points, and find we require a minimum window width of 60° longitude. Decreasing the window width to 90° and 60° (Figs 11b and c) results in changing from one highly anisotropic western region and one low anisotropic eastern region (Fig. 11a) to three regions with distinct anisotropy (Fig. 11c). We find a region with strong anisotropy of 3-4 per cent between 110°W and 40°W, moderate anisotropy of 2 per cent between 30°W and 75°E, and a broad region of low anisotropy of 0.5 per cent between 100°E and 170°W. Increasing the amplitude of the mantle corrections once again only affects the highly anisotropic region, further outlining how the mantle corrections preferentially affect the SSI data. Interestingly however, even when the SSI are not included in this analysis (the black line) there is still a recognizable increase in anisotropy around 100°W. This sharp peak cannot be seen in Fig. 11(a), where the window width is much larger masking this smaller feature. This shows that even without the SSI a region of higher anisotropy in the west is still required by the data. This analysis represents an increase in resolution when it comes to identifying inner core structure and is a direct result of an increase in polar and ultra-polar data.

4.2 Variations with depth

It has been hypothesized that there is an innermost inner core with a distinct anisotropic structure (Ishii & Dziewoński 2002; Beghein & Trampert 2003; Ishii & Dziewoński 2003; Sun & Song 2008a; Wang *et al.* 2015; Wang & Song 2018), although this is an open question as some researches also find a lack of evidence for an innermost inner core (Cormier & Stroujkova 2005; Lythgoe *et al.* 2014; Romanowicz & Mitchell 2015; Frost & Romanowicz 2019). An innermost inner core was originally inferred by Ishii & Dziewoński (2002) who proposed a region with 300 km radius and a slow axis with an angle of 45° to the fast direction. To investigate the potential evidence of an innermost inner core, we conduct a misfit analysis on our data set, splitting the data in two layers based on the radius of the turning point of each ray path and calculating anisotropy and misfit for both subsets of data. Fig. 12 shows the results of this analysis including the SSI data. Comparing the variation of misfit with layer radius (Fig. 12b) and the histogram showing the numbers of data for each radius (Fig. 12a) it can be seen that the lowest misfit comes from a layer with a radius of 947 km, which corresponds to the maximum

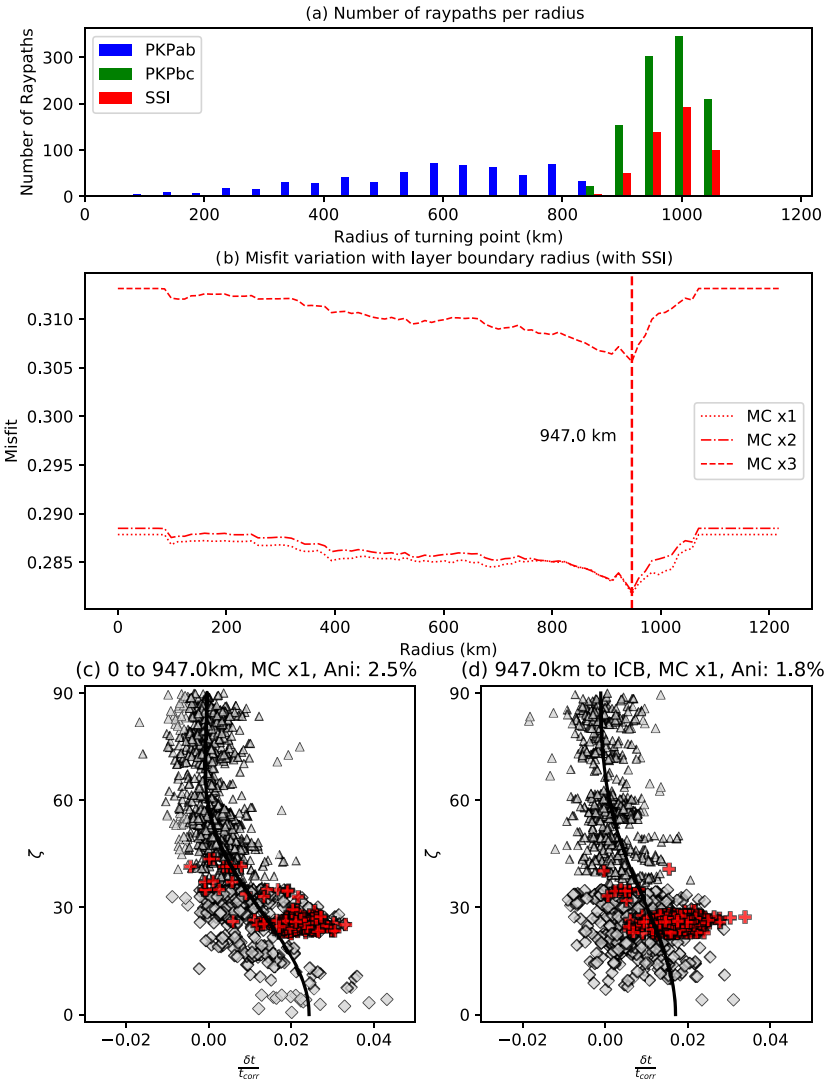

Figure 12. (a) Histogram showing the numbers of data observed for each turning point radius. When both PKPbc and PKPab phases are observed only the PKPbc observation is used in misfit and anisotropy calculations. (b) The variation of misfit with boundary radius used to separate data into two, for varying magnitude of the mantle corrections (x1,x2,x3). The vertical dashed line denotes the radius with the minimum misfit and (c and d) the corresponding plots of $\delta t/t$ against ζ for data with a turning point radius between 0 and 947 km and between 947 km (the minimum misfit boundary found by all data) and the inner core boundary, respectively.

depth extent of the SSI data which mostly travel the top 300 km of the inner core. This shows that the large anomalous SSI data set is masking deeper structure and misfit reductions. While most SSI data travel the upper 300 km, there are also some SSI data (shown in Fig. 12c) which travel deeper in the inner core between a radius of 450 and 947 km.

To be able to see any further misfit reductions we repeat the analysis with the SSI data removed (Fig. 13). The variation of misfit with layer radius for a data set with no SSI ray paths has a misfit minima at a radius of 690 km (or 530 km below the inner core boundary) (Fig. 13b). We find that the innermost inner core is significantly more anisotropic (Fig. 13c). In contrast to Ishii & Dziewoński (2002) the slow direction appears to be perpendicular to the direction of fastest velocity which is still aligned with Earth's axis of rotation and our innermost inner core is 690 km in radius, much larger than their 300 km, but in better agreement with values proposed from the recent study by Frost & Romanowicz (2019). The ultra-polar data which travels through the innermost inner core spans a large range of longitudes and there appears to be no justification for hemispherical variations within the innermost inner core. For the analysis in Section 4.3 we keep this value of 690km radius for the depth boundary.

It is interesting to see that increasing the strength of the mantle corrections show the same pattern of misfit with layer radius but that stronger mantle corrections increase overall misfit (although not significantly Figs 12b and 13b). This can be seen in Fig. 7, where the overall trend of the mantle corrections is to decrease the $\delta t/t$ anomaly of the SSI data, but that some SSI paths are not affected creating a slightly larger overall misfit.

4.3 Preliminary 3-D model of the inner core

We combined our findings on longitudinal variations (Fig. 11) and variations with depth (Fig. 13) to make a preliminary model of inner

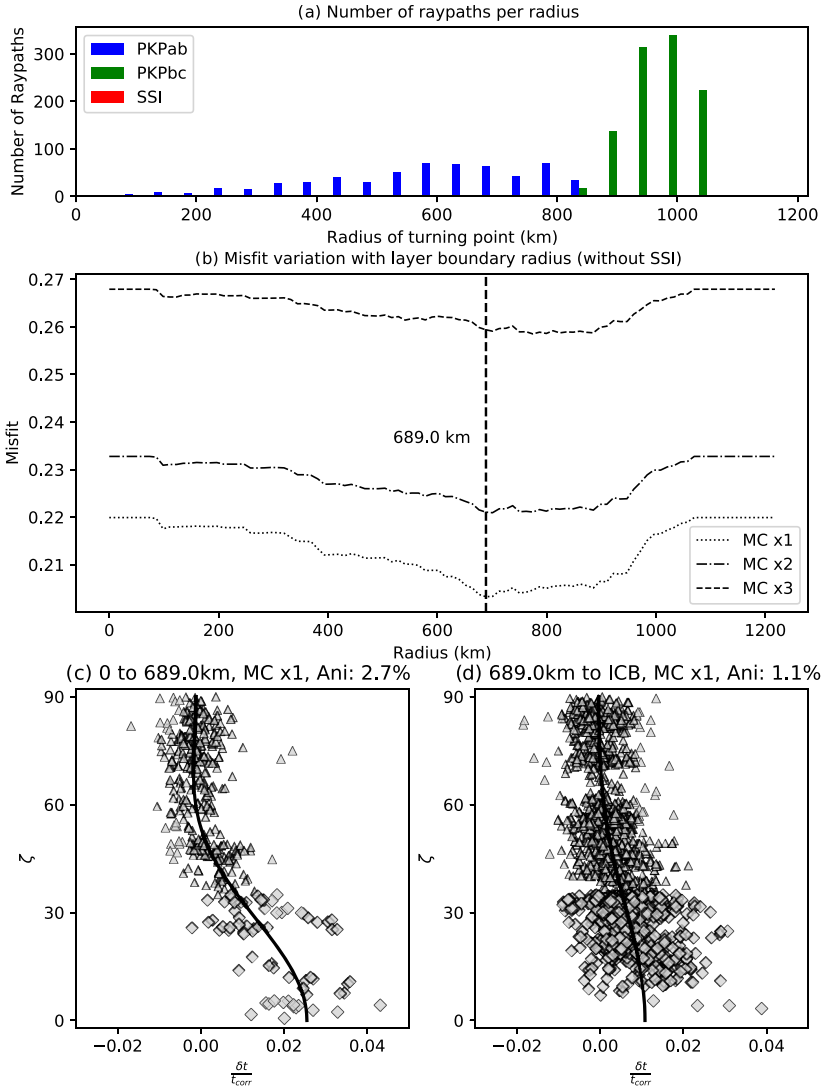

Figure 13. (a) Histogram showing the numbers of data observed for each turning point radius. When both PKPbc and PKPab phases are observed in the same seismogram, then only the PKPbc observation is used in misfit and anisotropy calculations. This analysis does not include data from the SSI. (b) The variation of misfit with boundary radius used to separate data into two, for varying magnitude of the mantle corrections (x1,x2,x3). The vertical dashed line denotes the radius with the minimum misfit and (c and d) the corresponding plots of $\delta t/t$ against ζ for data with a turning point radius between 0 and 690 km and between 690 km (the minimum misfit boundary found by all data) and the inner core boundary, respectively.

core anisotropy using data (including SSI) which has been mantle corrected with UUP07 velocities and also including ray path corrections (Fig. 14). The anisotropy variations are determined by fitting eq. (3) to data with turning point locations within each region. Like the results in the previous two sections, this is meant only as an initial estimate to be built upon with future research. Our model includes an innermost inner core with a radius of 690 km which is a homogeneous region of strong anisotropy (around 2.7 per cent). In the layer above there is longitudinal heterogeneity separated into three regions: region I with strong anisotropy up to 3.4 per cent, a transition region II with 1.4 per cent anisotropy and region III with weak anisotropy of 0.9 per cent. Visually comparing Figs 14(a) and (b) shows a clear correspondence between regions of stronger anisotropy and regions where the polar data is faster. Given the large uncertainty over the source of the anomalous SSI differential traveltimes, we show the same regional model but with the SSI data removed in Fig. 15. The main difference is that in region I, which contained the majority of the SSI data, the anisotropy is reduced from 3.4 to 2.8 per cent and in the IMIC it is reduced from 2.7 to 2.6 per cent. The overall structure has not changed when removing the SSI data; there are still regions with stronger anisotropy in the west and centre and low anisotropy elsewhere, only the magnitudes have changed. The corresponding models for stronger mantle corrections are given in the Supporting Information (Figs S2 and S3) and show the same features.

5 CONCLUSION

We present a new high-quality differential arrival data set for inner core *P*-wave phases containing a large number of polar data not originating in the SSI taking advantage of new stations in the Antarctic. The addition of ultra-polar paths allows us to more reliably determine inner core anisotropy because extrapolation to

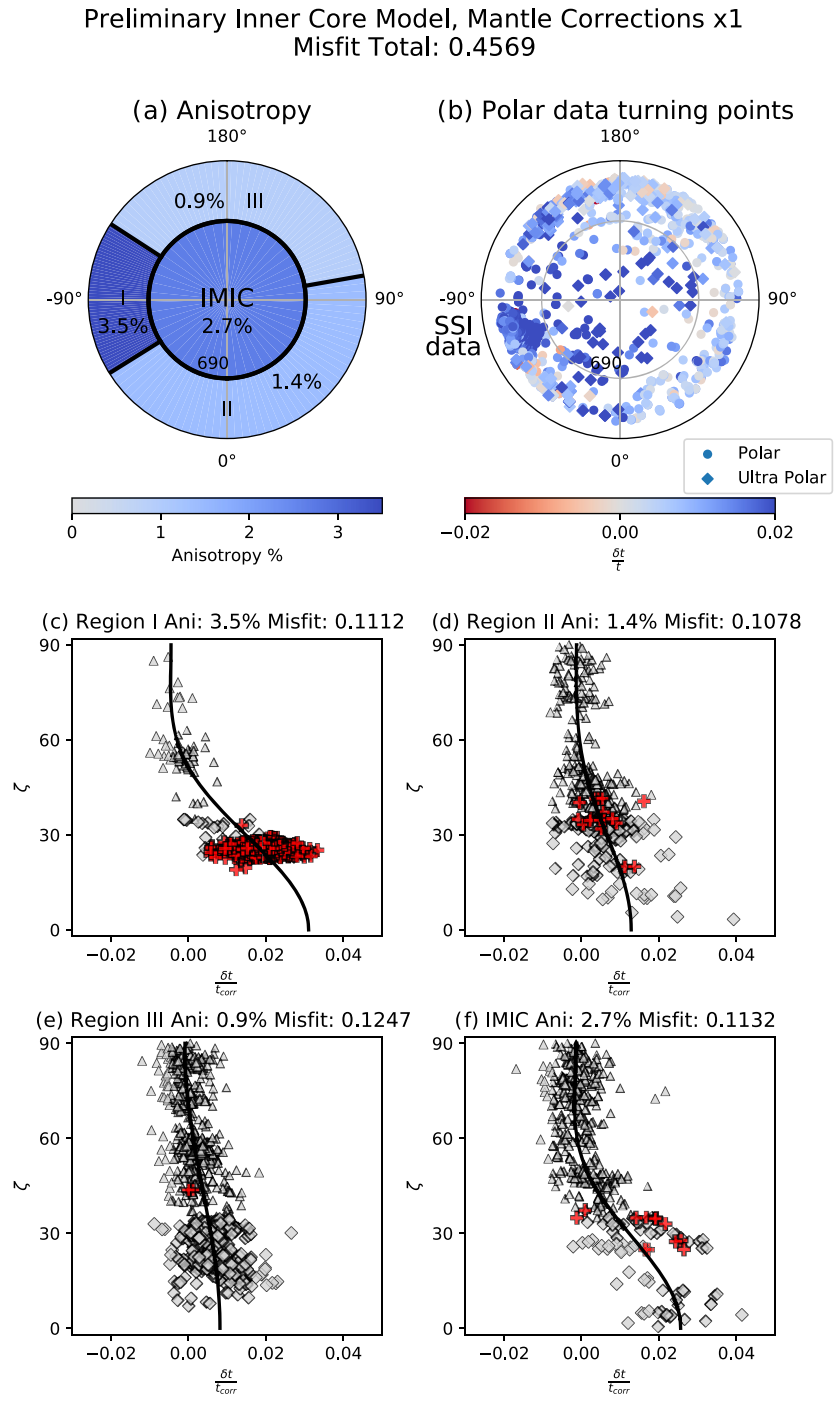

Figure 14. (a) A slice through the equatorial plane showing our preliminary model for inner core anisotropy with three regions between 690 km and the inner core boundary and one innermost inner core with a radius of 690 km with mantle corrected data using original UUP07 velocities (x1). (b) Polar data plotted at their turning points with colour representing the $\delta t/t$ anomaly. (c–f) Variation of $\delta t/t$ against ζ for our data set split into the regions defined by the model (a). The same figure but for our data set with mantle corrections x2 with the SSI data and x3 with the SSI data can be found in the Supporting Information (Figs S2 and S3).

small ζ is no longer required. We demonstrate that mantle structure and ray path changes have a larger effect on the anomalous SSI data than the other data, due to their short epicentral distances and large travel time anomalies. Our anisotropy values for the whole inner core including mantle and ray path correction range between 1.9 and 2.3 per cent, which is significantly lower than previously published research. Furthermore, our anisotropy models constructed from body wave data sensitive to shallow structure are in better agreement with normal mode measurements of inner core anisotropy sensitive to similar depths. Our new data still requires longitudinal and depth variations; we find a four-region model with an innermost inner core and an outer inner core with longitudinal heterogeneity in three different regions can be resolved by the data.

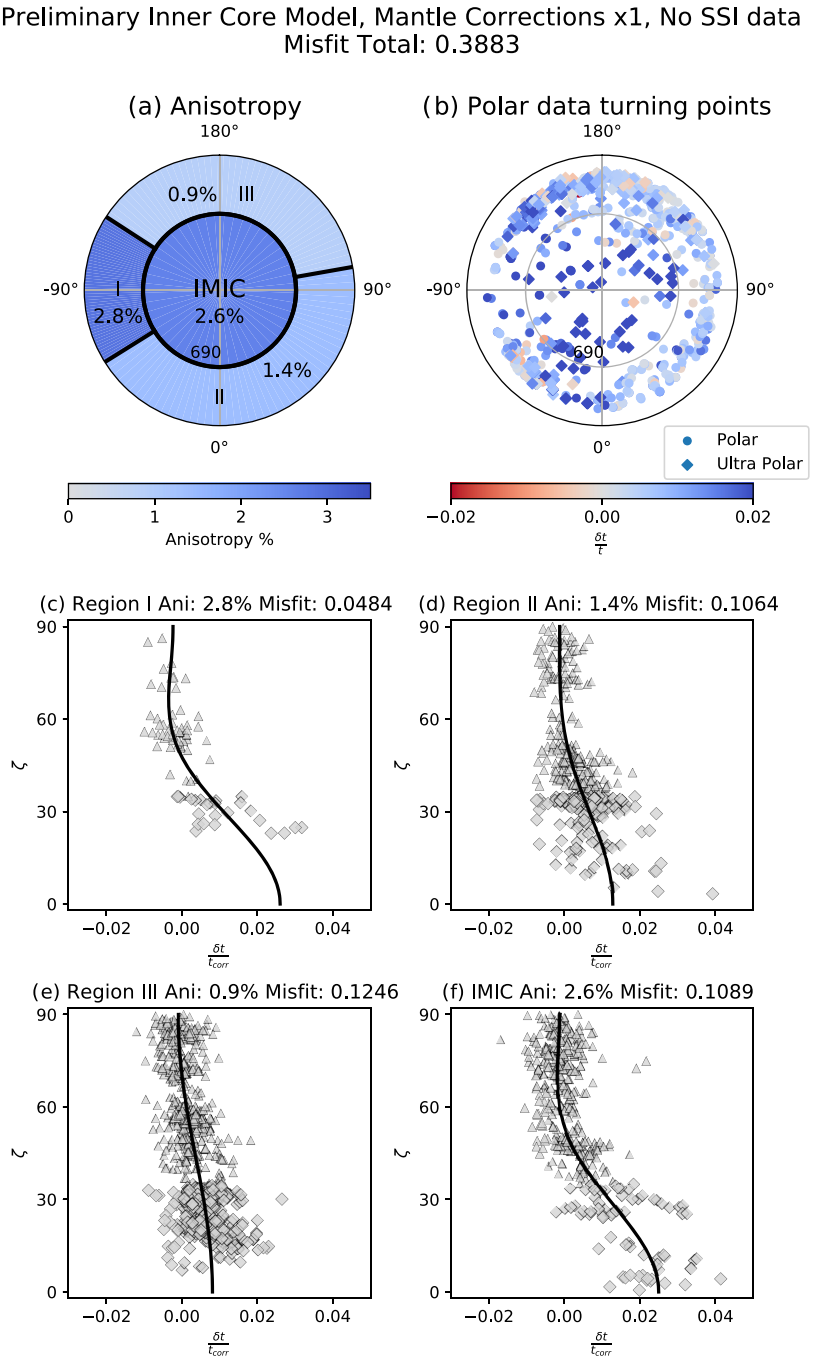

Figure 15. (a) A slice through the equatorial plane showing our preliminary model for inner core anisotropy with three regions between 690 km and the inner core boundary and one innermost inner core with a radius of 690 km with mantle corrected data using original UUP07 velocities (x1) but without the SSI data. (b) Polar data plotted at their turning points with colour representing the $\delta t/t$ anomaly. (c–f) Variation of $\delta t/t$ against ζ for our data set split into the regions defined by the model (a).

ACKNOWLEDGEMENTS

This research was supported by the European Research Council (ERC) under the European Union's Horizon 2020 Framework Programme (grant agreement No. 681535—ATUNE) and a Vici award number 016.160.310/526 from the Nederlandse Organisatie voor Wetenschappelijk Onderzoek (NWO). Special thanks to Prof. Wim Spakman for providing the tomographic model UUP07 and help with the theory of path integration necessary to conduct mantle corrections. The facilities of IRIS Data Services, and specifically the IRIS Data Management Center, were used for access to waveform, metadata or products required in this study. The IRIS DS is funded through the National Science Foundation and specifically the GEO Directorate through the Instrumentation and Facilities Program of the National Science Foundation under Cooperative Agreement EAR-1063471. Some activities are supported by the

National Science Foundation EarthScope Program under Cooperative Agreements EAR-0733069, EAR-1261681. While too many networks were used to acknowledge them all along their institutions individually, a number of networks were of special note as they recorded the ultra-polar data at the core of this research; TA, ZM, YT, II, AI, IU, G, AU, XF, XD, CN, XH, DK, GE, YE. Data processing was done using the Obspy and Scipy python packages. Data is available upon request from the first author via email.

REFERENCES

Amaru, M.L., 2007. Global travel time tomography with 3-D reference models, *PhD thesis*, Utrecht University, http://www.igitur.nl/.

Beghein, C. & Trampert, J., 2003. Robust normal mode constraints on inner-core anisotropy from model space search, *Science,* **299**(5606), 552–555.

Brëger, L., Tkalčić, H. & Romanowicz, B., 2000. The effect of D″ on PKP(AB–DF) travel time residuals and possible implications for inner core structure, *Earth planet. Sci. Lett.,* **175**(1–2), 133–143.

Cormier, V.F. & Stroujkova, A., 2005. Waveform search for the innermost inner core, *Earth planet. Sci. Lett.,* **236**(1–2), 96–105.

Creager, K.C., 1992. Anisotropy of the inner core from differential travel times of the phases PKP and PKIKP, *Nature,* **356**(6367), 309–314.

Creager, K.C., 1999. Large-scale variations in inner core anisotropy, *J. geophys. Res.,* **104**(B10), 23 127–23 139.

Crotwell, H.P., Owens, T.J. & Ritsema, J., 1999. The TauP toolkit: flexible seismic travel-time and ray-path utilities, *Seismol. Res. Lett.,* **70,** 154–160.

Deuss, A., 2014. Heterogeneity and anisotropy of Earth's inner core, *Annu. Rev. Earth Planet. Sci.,* **42,** 103–126.

Deuss, A., Irving, J.C. & Woodhouse, J.H., 2010. Regional variation of inner core anisotropy from seismic normal mode observations, *Science,* **328**(5981), 1018–1020.

Dziewonski, A.M. & Gilbert, F., 1976. The effect of small, aspherical perturbations on travel times and a re-examination of the corrections for ellipticity, *Geophys. J. R. astr. Soc.,* **44**(1), 7–17.

Frost, D.A. & Romanowicz, B., 2019. On the orientation of the fast and slow directions of anisotropy in the deep inner core, *Phys. Earth planet. Inter.,* **286,** 101–110.

Frost, D.A., Romanowicz, B. & Roecker, S., 2020. Upper mantle slab under Alaska: contribution to anomalous core-phase observations on south-Sandwich to Alaska paths, *Phys. Earth planet. Inter.,* **299,** 106427, doi:10.1016/j.pepi.2020.106427.

Garcia, R., 2002. Constraints on upper inner-core structure from waveform inversion of core phases, *Geophys. J. Int.,* **150**(3), 651–664.

Garcia, R. & Souriau, A., 2000. Inner core anisotropy and heterogeneity level, *Geophys. Res. Lett.,* **27**(19), 3121–3124.

Garcia, R., Tkalčić, H. & Chevrot, S., 2006. A new global PKP data set to study earth's core and deep mantle, *Phys. Earth planet. Inter.,* **159**(1–2), 15–31.

Gubbins, D., Willis, A.P. & Sreenivasan, B., 2007. Correlation of Earth's magnetic field with lower mantle thermal and seismic structure, *Phys. Earth planet. Inter.,* **162**(3–4), 256–260.

Hollerbach, R. & Jones, C.A., 1995. On the magnetically stabilizing role of the earth's inner core, *Phys. Earth planet. Inter.,* **87**(3–4), 171–181.

Irving, J. & Deuss, A., 2011. Hemispherical structure in inner core velocity anisotropy, *J. geophys. Res.,* **116**(B4), doi:10.1029/2010JB007942.

Ishii, M. & Dziewoński, A.M., 2002. The innermost inner core of the Earth: evidence for a change in anisotropic behavior at the radius of about 300 km, *Proc. Natl. Acad. Sci. USA,* **99**(22), 14 026–14 030.

Ishii, M. & Dziewoński, A.M., 2003. Distinct seismic anisotropy at the centre of the Earth, *Phys. Earth planet. Inter.,* **140**(1–3), 203–217.

Isse, T. & Nakanishi, I., 2002. Inner-core anisotropy beneath Australia and differential rotation, *Geophys. J. Int.,* **151**(1), 255–263.

Kennett, B., Engdahl, E. & Buland, R., 1995. Constraints on seismic velocities in the Earth from traveltimes, *Geophys. J. Int.,* **122**(1), 108–124.

Koketsu, K. & Sekine, S., 1998. Pseudo-bending method for three-dimensional seismic ray tracing in a spherical Earth with discontinuities, *Geophys. J. Int.,* **132**(2), 339–346.

Lehmann, I., 1936. P', *Publ. Bur. Cent. Seismol. Int. Ser. A,* **14,** 87–115.

Leykam, D., Tkalčić, H. & Reading, A.M., 2010. Core structure re-examined using new teleseismic data recorded in Antarctica: evidence for, at most, weak cylindrical seismic anisotropy in the inner core, *Geophys. J. Int.,* **180**(3), 1329–1343.

Long, X., Kawakatsu, H. & Takeuchi, N., 2018. A sharp structural boundary in lowermost mantle beneath Alaska detected by core phase differential travel times for the anomalous South Sandwich Islands to Alaska path, *Geophys. Res. Lett.,* **45**(1), 176–184.

Love, A., 1927. *A Treatise on the Mathematical Theory of Elasticity* , Cambridge University Press.

Lythgoe, K., Deuss, A., Rudge, J. & Neufeld, J., 2014. Earths inner core: innermost inner core or hemispherical variations? *Earth planet. Sci. Lett.,* **385,** 181–189.

Morelli, A., Dziewonski, A.M. & Woodhouse, J.H., 1986. Anisotropy of the inner core inferred from PKIKP travel times, *Geophys. Res. Lett.,* **13**(13), 1545–1548.

Niu, F. & Wen, L., 2001. Hemispherical variations in seismic velocity at the top of the Earth's inner core, *Nature,* **410**(6832), 1081–1084.

Olson, P., Christensen, U. & Glatzmaier, G.A., 1999. Numerical modeling of the geodynamo: mechanisms of field generation and equilibration, *J. geophys. Res.,* **104**(B5), 10 383–10 404.

Oreshin, S. & Vinnik, L., 2004. Heterogeneity and anisotropy of seismic attenuation in the inner core, *Geophys. Res. Lett.,* **31**(2), doi:10.1029/2003GL018591.

Poupinet, G., Pillet, R. & Souriau, A., 1983. Possible heterogeneity of the Earth's core deduced from PKIKP travel times, *Nature,* **305**(5931), 204–206.

Romanowicz, B. & Mitchell, B., 2015. 1.25—deep earth structure: *Q* of the Earth from crust to core, in *Treatise on Geophysics,* Vol. 1, pp. 789–827, ed. Schubert, G., Elsevier.

Romanowicz, B. & Wenk, H.-R., 2017. Anisotropy in the deep Earth, *Phys. Earth planet. Inter.,* **269,** 58–90.

Romanowicz, B., Tkalcic, H. & Breger, L., 2003. On the origin of complexity in PKP travel time data, in *Earth's Core: Dynamics, Structure, Rotation,* Vol. 31, pp. 31–44, eds Dehant, V., Creager, K.C., Karato, S.-I. & Zatman, S., doi:10.1029/GD031p0031.

Shearer, P.M. & Toy, K.M., 1991. PKP (BC) versus PKP (DF) differential travel times and aspherical structure in the Earth's inner core, *J. geophys. Res.,* **96**(B2), 2233–2247.

Song, X. & Richards, P.G., 1996. Seismological evidence for differential rotation of the Earth's inner core, *Nature,* **382**(6588), 221–224.

Su, W.-J. & Dziewonski, A.M., 1995. Inner core anisotropy in three dimensions, *J. geophys. Res.,* **100**(B6), 9831–9852.

Sun, X. & Song, X., 2008a. The inner inner core of the Earth: texturing of iron crystals from three-dimensional seismic anisotropy, *Earth planet. Sci. Lett.,* **269**(1–2), 56–65.

Sun, X. & Song, X., 2008b. Tomographic inversion for three-dimensional anisotropy of Earth's inner core, *Phys. Earth planet. Inter.,* **167**(1–2), 53–70.

Tanaka, S. & Hamaguchi, H., 1997. Degree one heterogeneity and hemispherical variation of anisotropy in the inner core from PKP (BC)–PKP (DF) times, *J. geophys. Res.,* **102**(B2), 2925–2938.

Tkalčić, H., 2010. Large variations in travel times of mantle-sensitive seismic waves from the South Sandwich Islands: is the Earth's inner core a conglomerate of anisotropic domains? *Geophys. Res. Lett.,* **37**(14), doi:10.1029/2010GL043841.

Tkalčić, H., 2015. Complex inner core of the Earth: the last frontier of global seismology, *Rev. Geophys.,* **53**(1), 59–94.

van der Meer, D.G., van Hinsbergen, D.J. & Spakman, W., 2018. Atlas of the underworld: slab remnants in the mantle, their sinking history, and a new outlook on lower mantle viscosity, *Tectonophysics,* **723,** 309–448.

Wang, T. & Song, X., 2018. Support for equatorial anisotropy of Earth's inner-inner core from seismic interferometry at low latitudes, *Phys. Earth planet. Inter.,* **276,** 247–257.

Wang, T., Song, X. & Xia, H.H., 2015. Equatorial anisotropy in the inner part of Earth's inner core from autocorrelation of earthquake coda, *Nat. Geosci.,* **8**(3), 224–227.

Waszek, L. & Deuss, A., 2011. Distinct layering in the hemispherical seismic velocity structure of Earth's upper inner core, *J. geophys. Res.,* **116**(B12), doi:10.1029/2011JB008650.

Wen, L. & Niu, F., 2002. Seismic velocity and attenuation structures in the top of the Earth's inner core, *J. geophys. Res.,* **107**(B11), ESE 2–1-ESE 2-13.

Woodhouse, J.H., Giardini, D. & Li, X.-D., 1986. Evidence for inner core anisotropy from free oscillations, *Geophys. Res. Lett.,* **13**(13), 1549–1552.

Yu, W. & Wen, L., 2006. Seismic velocity and attenuation structures in the top 400 km of the Earth's inner core along equatorial paths, *J. geophys. Res.,* **111**(B7), doi:10.1029/2005JB003995.

SUPPORTING INFORMATION

Supplementary data are available at *GJI* online.

Figure S1. This figure shows how the values of δt from the PKPab-PKPdf residual and the PKPbc-PKPdf residual vary for the same ray paths. The mean and standard deviation of the differences in the differential traveltimes are 0.3 and 0.7 s, respectively.

Figure S2. (a) Variation of $\delta t/t$ as a function of ζ for (a) PKPbc-PKPdf and (b) PKPab-PKPdf with the SSI data left out. The black line is the function described by eq. (3) fitted to the data with a least-squares norm. The triangles are equatorial data ($\zeta > 35^\circ$), diamonds are polar data (not including SSI). (c and (d) Variations of $\delta t/t$ against ζ applying mantle corrections using the UUP07 tomographic model. (e and f) Variation of $\delta t/t$ applying mantle and ray path corrections.

Figure S3. (a) A slice through the equatorial plane showing our preliminary model for inner core anisotropy with three regions between 690 km and the inner core boundary and one innermost inner core with a radius of 690 km with mantle corrected data using doubled UUP07 velocities (x2). (b) Polar data plotted at their turning points with colour representing the $\delta t/t$ anomaly. (c–f) Variation of $\delta t/t$ against ζ for our data set split into the regions defined by the model (a).

Figure S4. (a) A slice through the equatorial plane showing our preliminary model for inner core anisotropy with three regions between 690 km and the inner core boundary and one innermost inner core with a radius of 690 km with mantle corrected data using tripled UUP07 velocities (x3). (b) Polar data plotted at their turning points with colour representing the $\delta t/t$ anomaly. (c–f) Variation of $\delta t/t$ against ζ for our data set split into the regions defined by the model (a).

Please note: Oxford University Press is not responsible for the content or functionality of any supporting materials supplied by the authors. Any queries (other than missing material) should be directed to the corresponding author for the paper.